

## Spectroscopy and defect states in polyaniline

R. P. McCall, J. M. Ginder, J. M. Leng, and H. J. Ye  
*Department of Physics, The Ohio State University, Columbus, Ohio 43210-1106*

S. K. Manohar, J. G. Masters, G. E. Asturias, and A. G. MacDiarmid  
*Department of Chemistry, University of Pennsylvania, Philadelphia, Pennsylvania 19104-6323*

A. J. Epstein  
*Department of Physics and Department of Chemistry, The Ohio State University, Columbus, Ohio 43210-1106*  
 (Received 11 September 1989)

We report the far-infrared through visible photoinduced absorption (PA) spectra of polyaniline in the emeraldine-base and leucoemeraldine-base forms. The direct-absorption spectrum of emeraldine base (EB) has a broad absorption centered at 2 eV (the "exciton" band) and an absorption band at  $\sim 3.6$  eV (the  $\pi$ - $\pi^*$  band gap). The PA spectra of EB for pumping into the "exciton" band and across the band gap are nearly identical, indicating the same types of charged defect states are created upon photoexcitation. The direct absorption spectrum of leucoemeraldine base (LB) shows only the  $\pi$ - $\pi^*$  band-gap absorption at  $\sim 3.6$  eV. For pumping into this absorption band, the PA spectrum of LB is very similar to that of EB, although important differences result from the lack of quinoid structures in this material. Based on our results, we propose a model for the photocreation of defect states in leucoemeraldine base and emeraldine base. The central roles of phenyl-ring rotations and of massive polarons are discussed.

## I. INTRODUCTION

The study of conducting polymers has given rise to a number of important and novel concepts including the formation of defect states, such as solitons, polarons, and bipolarons, that describe many of the properties of these materials. One such conducting polymer, polyaniline, has been shown to have significantly different properties than earlier studied materials, such as polyacetylene and polythiophene.<sup>1</sup> Many of these properties arise from the alternating ring-heteroatom backbone structure and from the wide range of forms that polyaniline can have, depending on the number of electrons and protons on the polymer backbone.

The fully reduced leucoemeraldine base [LB, or poly(paraphenylene amine)] form of polyaniline, shown in Fig. 1, is an insulator whose large energy gap ( $E_g \sim 3.6$  eV) originates predominantly from extrinsic effects involving the overlap of molecular orbitals of neighboring phenyl rings and nitrogens.<sup>2</sup> LB is isoelectronic to other phenyl-ring-containing polymers such as poly(paraphenylene sulfide) (PPS) and poly(paraphenylene oxide) (PPO), but the presence of amine ( $-\text{NH}-$ ) groups allows chemical flexibility so that other electronic states of the polymer can be obtained by removal of protons or hydrogen atoms, as well as electrons, from the polymer. These other forms of polyaniline are determined by the fraction of imine ( $-\text{N}=\text{N}-$ ) nitrogens per four-ring repeat unit, which we label  $1-y$ . Thus, LB has a  $1-y$  value of zero. The half-oxidized ( $1-y = 0.5$ ) emeraldine base [EB, or poly(paraphenylene amine imine)] form of polyaniline (Fig. 1) is also an insulator with a large extrinsic gap ( $E_g \sim 3.6$  eV), similar to LB. In contrast to

LB and EB, the fully oxidized ( $1-y = 1$ ) pernigraniline base [PNB, or poly(paraphenylene imine)] form of polyaniline, shown in Fig. 1, has been proposed to have an energy gap ( $E_g \sim 1.4$  eV) that is intrinsic in origin<sup>3,4</sup> due to the electron-phonon interaction.

The conducting emeraldine salt (ES) form of polyaniline is achieved upon protonation of EB by exposure to protonic acids or upon oxidative doping of LB. In the conducting form, polyaniline supports the formation of polarons and can be described as possessing a metallic polaron energy band, resulting from a reorganization of the electronic structure. This description is supported by a number of theoretical and experimental studies.<sup>1,2,5-7</sup>

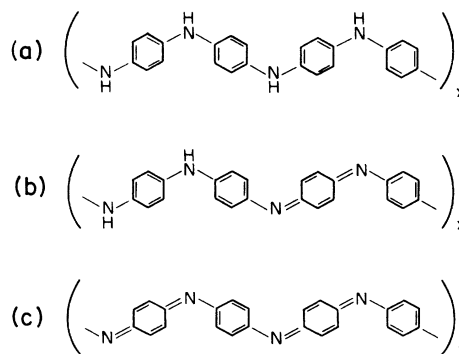


FIG. 1. (a) Leucoemeraldine base [ $-(\text{C}_{24}\text{H}_{20}\text{N}_4)_x-$ ], (b) emeraldine base [ $-(\text{C}_{24}\text{H}_{18}\text{N}_4)_x-$ ], and (c) pernigraniline base [ $-(\text{C}_{24}\text{H}_{16}\text{N}_4)_x-$ ].

Recent photoinduced-absorption (PA) studies<sup>8–12</sup> have shown that polarons can also be produced upon photoexcitation of the insulating EB polymer. The photoexcited polarons are massive ( $M_{\text{polaron}} > 60m_e$ , where  $M_{\text{polaron}}$  is the polaron mass and  $m_e$  is the electron mass) and have very long lifetimes ( $\tau > 2$  h at 80 K).<sup>8,9</sup> The presence of this long-lived photoinduced absorption has been suggested as a basis for erasable optical information storage technology.<sup>13</sup>

Investigations of electronic structure and defect states in polyaniline<sup>14–18</sup> have recognized the importance of phenyl-ring rotations in determining the ground-state and excited-state properties of these materials. For phenyl rings *in* the plane formed by the nitrogens, there is substantial energy gain due to delocalization of the  $\pi$  electrons. However, repulsive steric interactions between adjacent phenyl rings favor ring conformations *out* of the plane. Band-structure calculations<sup>15,17</sup> assume that the ground state in LB consists of neighboring phenyl rings rotated by equal but opposite angles *away* from the nitrogen-nitrogen plane. The presence of a hole polaron centered on a phenyl ring causes this ring and its neighboring rings to distort away from the ground-state configuration toward a more planar one.<sup>15</sup> Other excitations also involve changes in ring conformation.<sup>15</sup>

These ring-rotational defects are predicted to be quite massive<sup>15</sup> because of the large ring-angle distortions required for translational motion. The extremely long lifetimes observed in the PA spectra<sup>8,9</sup> may be a consequence of this large mass, but may also be due to chain packing in which the rotated phenyl rings are inhibited from relaxing back to their ground state by interactions with neighboring chains. At higher temperatures, thermally activated ring relaxations are possible,<sup>19</sup> which account for the temperature dependence of the lifetimes.<sup>8,9</sup>

It is important to determine the electronic structure and the various excited-state and defect-state configurations in polyaniline in order to understand the origins of the unusual physical properties observed in this family of materials. To investigate these electronic excitations, we have made measurements of the infrared and optical absorption spectra and photoinduced-absorption spectra of the leucoemeraldine base and emeraldine base forms of polyaniline. The optical absorption spectra of LB and EB show a  $\pi$ - $\pi^*$  band-gap absorption at  $\sim 3.6$ – $3.8$  eV, with an additional broad “excitation” absorption at 2 eV in EB. The infrared spectra are interpreted in terms of normal modes of *para*-disubstituted benzene. These optical and infrared absorption spectra are also used to determine the oxidation state of the polymer.

The photoinduced-absorption spectra of EB in the infrared and visible regions for pumping into the  $\pi$ - $\pi^*$  transition at 3.8 eV is reported and compared to previously reported data for pumping near 2.5 eV into the “exciton” band. The similarity of the data for these two pumping energies indicates that the same types of defect states are created upon photoexcitation. We also report PA spectra of LB for pumping across the  $\pi$ - $\pi^*$  band gap (at 3.8 eV) and compare our results to those obtained in EB. Again, the similarity of the data indicates that photoexcitation

of LB results in the formation of very similar defect states as in EB. On the basis of our results, we propose a scheme for the generation and evolution of defect states in polyaniline. These defect states include benzenoid and quinoid moieties that contain electrons or holes and involve the formation of trapped states near quinoid sites. New ring conformations are expected to accompany the formation of these defect states.

In the next section of this paper, we describe the experimental techniques used in this study, while in Sec. III, we present our experimental results for both direct absorption and photoinduced-absorption experiments. The data are discussed in Sec. IV and a model for the ground- and excited-state properties of polyaniline is proposed in Sec. V. A summary of our work is presented in the final section.

## II. EXPERIMENTAL TECHNIQUES

Samples of emeraldine base and leucoemeraldine base were prepared using previously described methods.<sup>20,21</sup> For the direct absorption measurements in the near-ir, visible, and ultraviolet regions, samples were dissolved in *N*-methyl pyrrolidinone (NMP) or were cast as thin films ( $\leq 0.5$   $\mu\text{m}$ ) from solution onto either glass or quartz substrates. (For EB, this procedure resulted in the EB-II form.<sup>22</sup>) These thin films were also used for the photoinduced-absorption experiments in the near-ir and visible regions. For direct absorption and photoinduced-absorption measurements in the near- to far-ir, powder material was mixed with KBr ( $\leq 0.1\%$  by weight) and pressed under vacuum into uniform, partly transparent pellets. (The EB powder used was obtained by treating as-synthesized emeraldine hydrochloride salt with  $\text{NH}_4\text{OH}$ , resulting in the EB-I form.<sup>22</sup>) Samples were attached to the end of a closed-cycle helium refrigerator, a continuous-flow liquid-helium refrigerator, or a liquid-nitrogen cold finger for measurements at low temperatures. The LB samples were kept in an inert environment throughout all stages of handling, while the EB samples were exposed to air at some point in the procedure. Thus, the EB samples are expected to be slightly overoxidized ( $1 - y \approx 0.56$ ).<sup>23</sup>

The direct absorption spectra were measured with a Perkin-Elmer Lambda 9 UV/Visible/NIR spectrophotometer in the range 900–250 nm (1.4–5.0 eV) or using a grating monochromator in the range 0.3–6 eV. In the near-ir to far-ir ( $500$ – $16\,000$   $\text{cm}^{-1}$ , 0.06–2.0 eV), a Nicolet 60SX FTIR spectrometer was used.

The photoinduced-absorption measurements were performed using two different experimental apparatus yielding results in different time domains and different (but overlapping) energy ranges. In the near-ir to near-uv range (0.5–3.5 eV), a near-steady-state apparatus based on the grating monochromator was used, which allowed time-dependent studies of the absorption and bleaching peaks in the millisecond range. In the mid- to near-ir range, the FTIR spectrometer was used, which allowed monitoring of the photoinduced infrared-active vibrations (IRAV) and higher-lying peaks for long times (up to 2 h or longer).

The near-steady-state photoinduced-absorption experiments were carried out using as a probe source the output of either a tungsten or deuterium lamp, which is focused onto the sample, filtered through a grating monochromator, and detected by the appropriate photodiodes. To photoexcite the sample, the output of either an argon-ion laser ( $E_{\text{pump}} \approx 2.4\text{--}2.7$  eV), a dye laser ( $E_{\text{pump}} \approx 2.0$  eV), or a mercury-xenon arc lamp with appropriate bandpass filters ( $E_{\text{pump}} \approx 3.8$  eV) was used. The pump beam was mechanically chopped at frequencies between 4 and 400 Hz, causing an induced change in the sample transmission,  $\Delta T$ . The uncorrected sample transmission,  $T$ , was measured simultaneously. The fractional change in transmission,  $-\Delta T/T$ , which is independent of the system response, was then computed. Because  $-\Delta T/T$  is proportional to the induced change in the absorption coefficient in the sample, increased absorption occurs when  $-\Delta T/T > 0$  and decreased absorption, or bleaching, occurs when  $-\Delta T/T < 0$ .

For the long time photoinduced-absorption measurements in the FTIR spectrometer, the probe beam was the output of either a Globar (mid-ir) or a tungsten lamp (near-ir), and the pump beam, again, was an argon-ion laser, a dye laser, or a mercury-xenon arc lamp as described above. The sample was first cooled to low temperatures in the dark, with neither the probe beam nor the pump beam incident on the sample. (The probe beam in the near-ir was observed to cause photoinduced changes in the sample spectra; exposure of the sample to the probe beam occurred only during data collection. For the mid-ir region, no photoinduced changes were observed as a result of exposure to the probe beam alone.) Next, the uncorrected transmission spectrum of the sample was measured, followed by photoexcitation by the pump source for a specified time. After blocking the pump beam, the transmission spectrum was measured immediately, and subsequently monitored for times up to 2 h. The fractional transmission change,  $-\Delta T/T$ , was determined from the difference in absorption *before* and *after* photoexcitation and is independent of the system response.

In photoinduced-absorption experiments, heating effects due to the pump source may cause induced changes in the absorption of the sample. Comparison of the near-steady-state PA spectra of LB and EB with temperature-dependent absorption measurements indicate that heating is not a factor in the data reported here. In the long time experiment, the PA spectra recorded immediately after turning the pump off were compared to spectra taken at later times, which demonstrated that no problems with heating occurred during the experiment.

### III. EXPERIMENTAL RESULTS

#### A. Direct absorption experiment

The uv/visible/near-ir direct absorption spectra of leucoemeraldine base and emeraldine base in solutions of NMP are shown in Fig. 2. The spectrum for LB reveals a strong absorption band centered at  $\sim 3.6$  eV. Thin-film data show this band close to  $\sim 3.8$  eV. In EB, the spec-

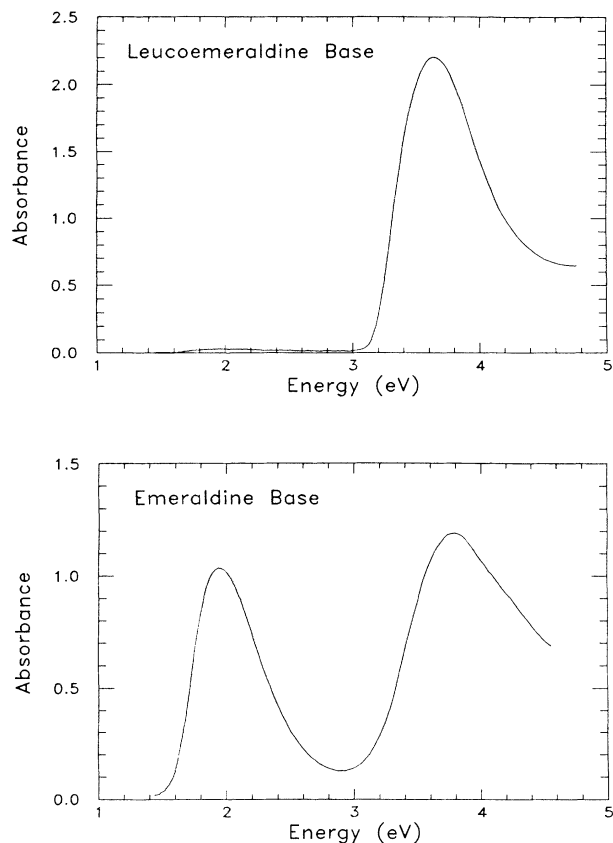


FIG. 2. UV/visible/near-ir absorption spectra of leucoemeraldine base (top) and emeraldine base (bottom) in solutions of NMP.

trum shows a very similar absorption band centered at  $\sim 3.8$  eV with an additional strong absorption centered at  $\sim 2.0$  eV. We note that though the spectrum of LB shows very little absorption below the 3.6-eV peak, there is a small residual absorption near 2 eV.

The infrared absorption spectra of powder samples of LB and EB in pressed KBr pellets are shown in Fig. 3. Strong vibrations are observed in LB at 816, 1284, 1497, and 1613  $\text{cm}^{-1}$  and in EB at 831, 1166, 1304, 1498, and 1592  $\text{cm}^{-1}$ . Other weaker vibrational modes are also observed.

#### B. Near-steady-state photoinduced absorption experiment

The near-steady-state photoinduced-absorption spectrum of emeraldine base in the range 0.5–3.5 eV is shown in Fig. 4 (top) for  $E_{\text{pump}} = 2.54$  eV at a chopper frequency of 21 Hz, an intensity of 250  $\text{mW}/\text{cm}^2$ , and at a sample temperature of 15 K. The spectrum shows three PA features at 0.9, 1.4, and 3.0 eV and two photoinduced bleaching (PB) features at 1.9 and 3.7 eV. The spectrum can be assigned to the formation of defect states within the gap, with a concomitant bleaching of transitions observed in direct absorption experiments.<sup>10</sup>

Figure 4 (bottom) presents the near-steady-state PA spectrum of EB for  $E_{\text{pump}} = 3.8$  eV at a chopper frequency of 22.5 Hz, an intensity of 100  $\text{mW}/\text{cm}^2$ , and a sample

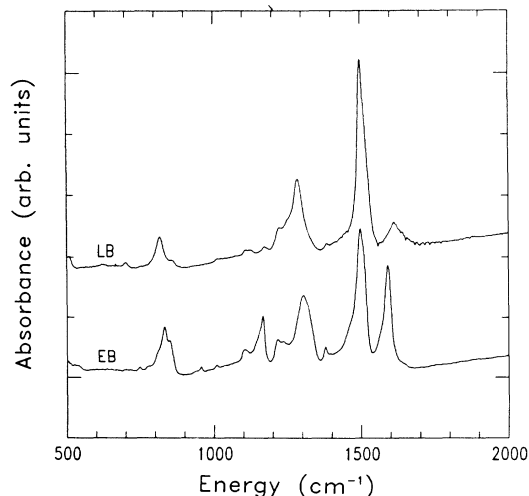


FIG. 3. Infrared absorption spectra of leucoemeraldine base (upper curve) and emeraldine base (lower curve) in pressed KBr pellets.

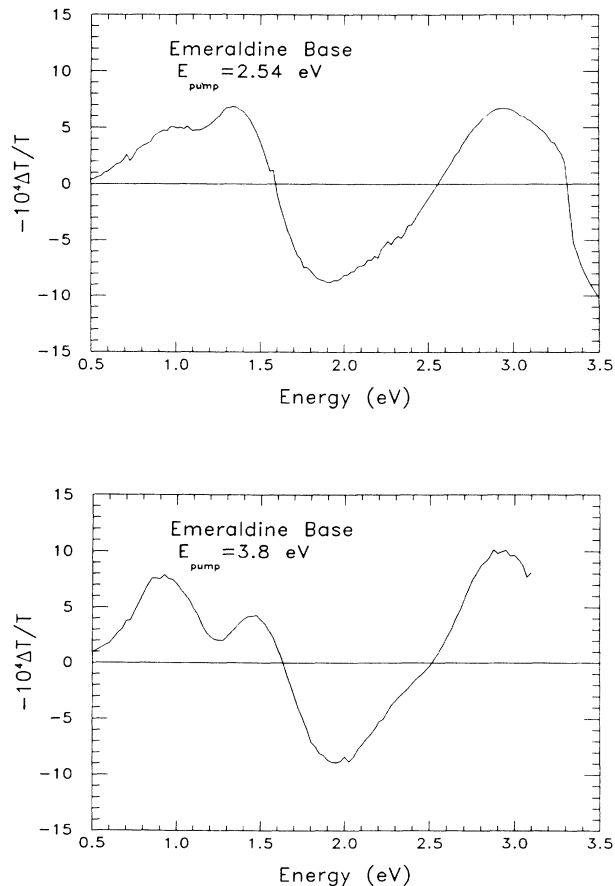


FIG. 4. Near-steady-state photoinduced-absorption spectra of a thin film of EB on quartz substrate at 15 K for  $E_{\text{pump}} = 2.54$  eV, pump intensity of  $250 \text{ mW/cm}^2$ , and chopper frequency of 21 Hz (top), and at 10 K for  $E_{\text{pump}} = 3.8$  eV, pump intensity of  $100 \text{ mW/cm}^2$ , and chopper frequency of 22.5 Hz (bottom).

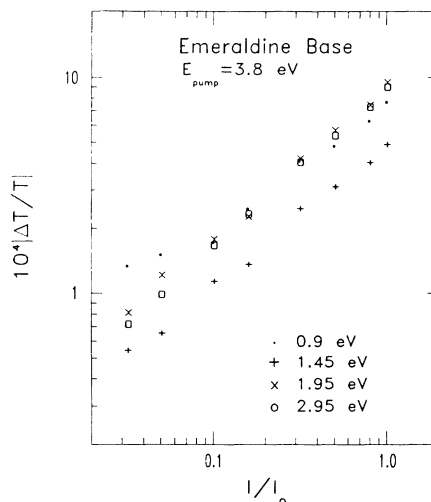


FIG. 5. Pump-intensity dependence of the four photoinduced features at 0.9, 1.45, 1.95, and 2.95 eV of a thin film of EB on a quartz substrate for a sample temperature of 10 K, pump energy of 3.8 eV, and chopper frequency of 22.5 Hz.  $I_0$  is  $130 \text{ mW/cm}^2$ .

temperature of 10 K. The same features are present for 3.8-eV pumping as for 2.54-eV pumping, which indicates that the same types of defect states are formed. The pump-intensity dependence of the PA and PB peaks in EB at 0.9, 1.4, 1.9, and 3.0 eV is shown in Fig. 5, and the chopper-frequency behavior of these peaks is shown in Fig. 6 for  $E_{\text{pump}} = 3.8$  eV. The pump-intensity and chopper-frequency dependence of the PA spectra of EB for  $E_{\text{pump}} \sim 2.5$  eV has been reported earlier.<sup>10</sup>

The near-steady-state PA spectra of leucoemeraldine base are shown in Fig. 7 for  $E_{\text{pump}} = 3.8$  eV, an intensity

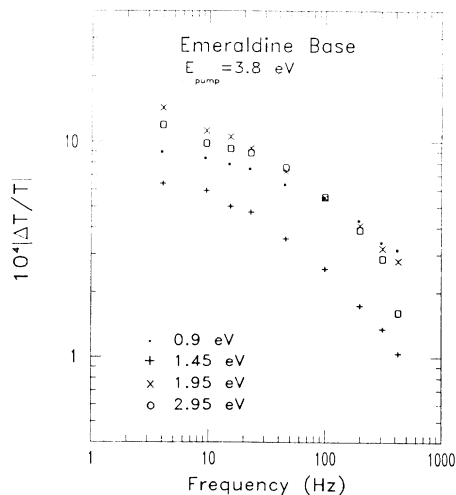


FIG. 6. Chopper-frequency dependence of the four photoinduced features at 0.9, 1.45, 1.95, and 2.95 eV of a thin film of EB on a quartz substrate for a sample temperature of 10 K, pump energy of 3.8 eV, and pump intensity of  $130 \text{ mW/cm}^2$ .

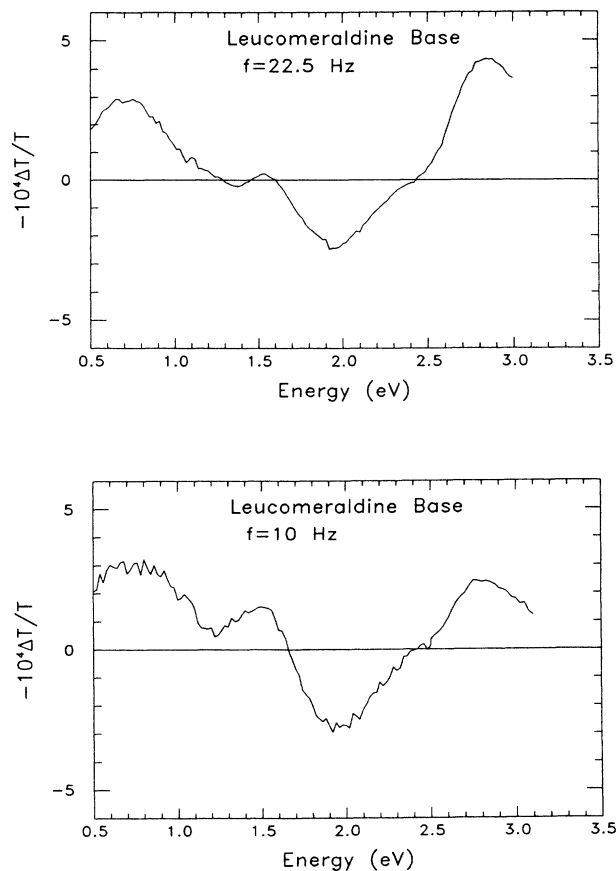


FIG. 7. Near-steady-state photoinduced-absorption spectra of a thin film of LB on a quartz substrate at 10 K with  $E_{\text{pump}} = 3.8$  eV, pump intensity of 190 mW/cm<sup>2</sup>, at chopper frequency 22.5 Hz (top) and 10 Hz (bottom).

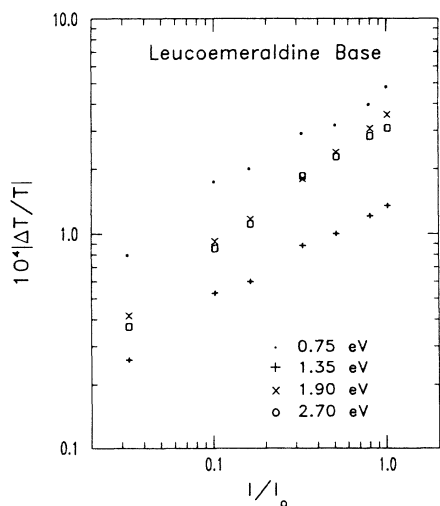


FIG. 8. Pump-intensity dependence of the four photoinduced features at 0.75, 1.35, 1.9, and 2.7 eV of a thin film of LB on a quartz substrate for a sample temperature of 10 K, pump energy of 3.8 eV, and chopper frequency of 22.5 Hz.  $I_0$  is 400 mW/cm<sup>2</sup>.

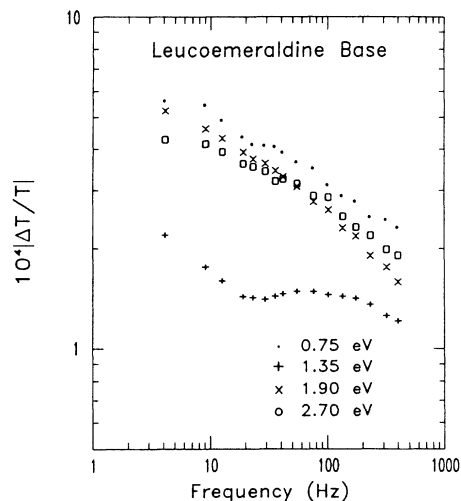


FIG. 9. Chopper-frequency dependence of the four photoinduced features at 0.75, 1.35, 1.9, and 2.7 eV of a thin film of LB on a quartz substrate for a sample temperature of 10 K, pump energy of 3.8 eV, and pump intensity of 200 mW/cm<sup>2</sup>.

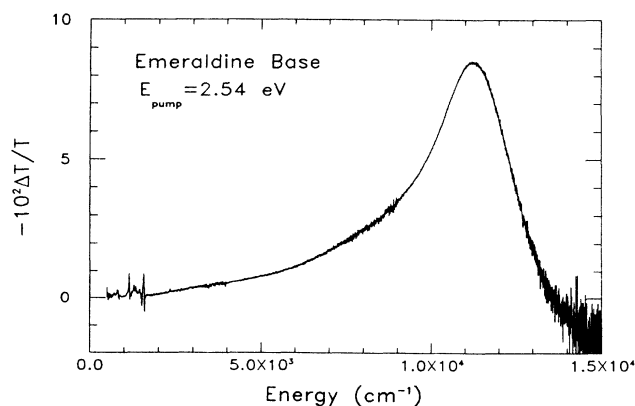
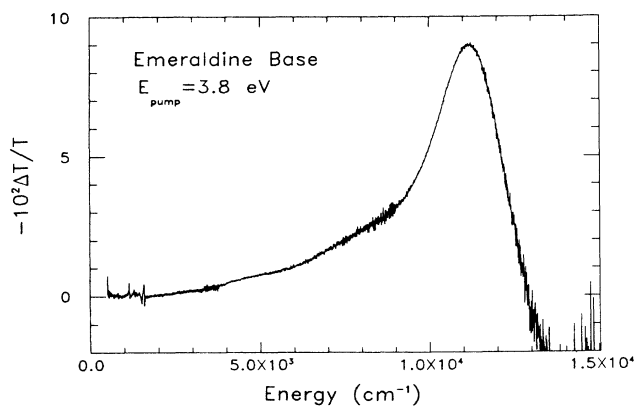


FIG. 10. Long time PA spectra of EB in KBr at 80 K for  $E_{\text{pump}} = 3.8$  eV (top) and  $E_{\text{pump}} = 2.54$  eV (bottom).

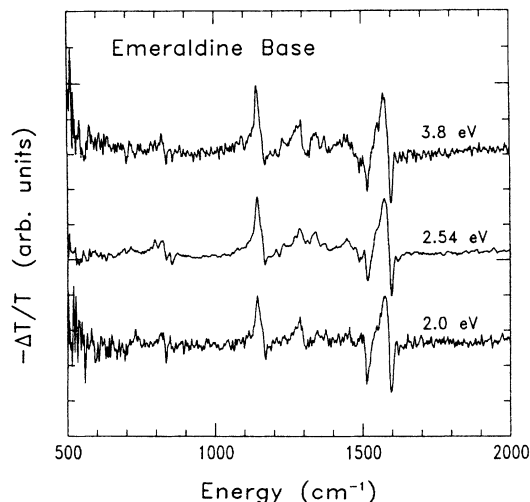


FIG. 11. Long time PA spectra in the mid-ir region of EB in KBr at 80 K for  $E_{\text{pump}} = 3.8$  eV (upper curve),  $E_{\text{pump}} = 2.54$  eV (middle curve), and  $E_{\text{pump}} = 2.0$  eV (lower curve).

of 190 mW/cm<sup>2</sup>, and a sample temperature of 10 K, for chopper frequencies of 22.5 Hz (top) and 10 Hz (bottom). PA peaks at 0.75 and 2.8 eV are quite strong, while the PA peak at  $\sim 1.4$  eV appears to have a strong frequency dependence at these low frequencies. Shown in Fig. 8 is the pump-intensity dependence of each of the PA and PB peaks in LB. Figure 9 shows the dependence of each peak on chopper frequency.

### C. Long-time photoinduced absorption experiment

The long time photoinduced-absorption spectra of emeraldine base in KBr in the range 500–15 000 cm<sup>-1</sup> are shown in Fig. 10 for 20-sec exposures at pump energies of 2.54 and 3.8 eV, intensities of 200 and 175 mW/cm<sup>2</sup>, respectively, and at a sample temperature of  $\sim 80$  K. Several photoinduced infrared-active vibrational (IRAV) modes are present, which are substantially weaker than the PA feature at  $\sim 1.4$  eV (11 200 cm<sup>-1</sup>). The photoin-

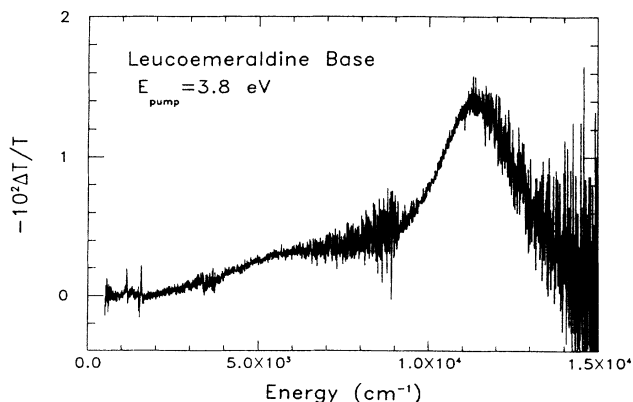


FIG. 12. Long time PA spectrum of LB in KBr at 80 K for pump energy  $E_{\text{pump}} = 3.8$  eV.

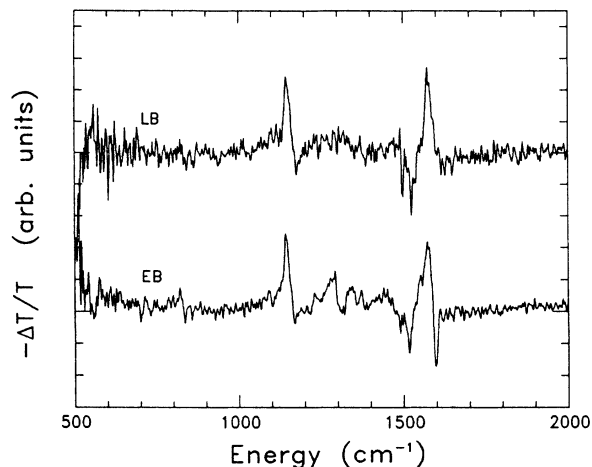


FIG. 13. Long time PA spectra in the mid-ir region of LB in KBr (upper curve) and EB in KBr (lower curve). For both spectra, the samples were held at 80 K and  $E_{\text{pump}} = 3.8$  eV.

duced IRAV modes are shown more clearly in Fig. 11 for 3.8- and 2.54-eV pumping and, in addition, 2.0-eV pumping at 180 mW/cm<sup>2</sup>. Major features include two PA peaks at 1144 and 1574 cm<sup>-1</sup> and two PB peaks at 1510 and 1599 cm<sup>-1</sup>. Other small photoinduced IRAV modes appear around 850 cm<sup>-1</sup> and in the range 1200–1400 cm<sup>-1</sup>. The PA spectra for  $E_{\text{pump}} = 2.0$ , 2.54, and 3.8 eV are nearly identical.

Shown in Fig. 12 is the long time PA spectrum of LB in KBr for  $E_{\text{pump}} = 3.8$  eV and a sample temperature of  $\sim 80$  K. The PA spectrum of LB shows the photoinduced IRAV modes in the mid-ir, a peak at 1.4 eV, and a new feature at  $\sim 0.75$  eV. The PA spectrum is quite similar to that of EB in Fig. 10, despite the presence of the 0.75-eV peak, even though its spectral intensity is weaker (and, consequently, noisier). Figure 13 compares the photoinduced IRAV modes of LB to those of EB where we again observe the similarity of the two spectra. In LB, however, we see two PA modes at 1144 and 1574 cm<sup>-1</sup>, but only one PB mode at 1510 cm<sup>-1</sup>.

The data shown in Figs. 10–13 represent the photoinduced changes that occurred in our samples immediately (within a measurement time of 5–10 s) after turning the pump beam off. Measurements of the spectra at later times (up to 2 h) revealed little or no decay of the PA signal at temperatures below 80 K. Above 150 K, the photoinduced features decayed at rates that increased with increasing temperatures.<sup>8,13</sup>

## IV. DISCUSSION OF EXPERIMENTAL RESULTS

### A. Direct absorption

The strong peak at  $\sim 3.6$  eV in the uv/visible/near-ir absorption spectrum of leucoemeraldine base, shown in Fig. 2, is the  $\pi$ - $\pi^*$  band-gap absorption in agreement with theoretical calculations.<sup>17</sup> The absorption spectrum of emeraldine base (Fig. 2) has an additional absorption that

peaks at  $\sim 2.0$  eV. This absorption band results from a charge-transfer excitonlike transition from the highest occupied energy levels (centered on the benzenoid rings) to the lowest unoccupied energy level (centered on the quinoid rings). Theoretical calculations<sup>14,16,17,24–26</sup> support this assignment. A very weak 2-eV peak is also observed in our LB samples indicating that there is a small fraction of quinoid groups present. Thus, the 2-eV peak can be used as a measure of the oxidation state of polyaniline.

The infrared spectrum of LB, shown in Fig. 3, can be described in terms of normal modes of *para*-disubstituted benzene, while the ir spectrum of EB includes additional modes associated with symmetry breaking of the benzenoids due to the presence of quinoid groups.<sup>8,9,27</sup> The vibrational mode at  $816\text{ cm}^{-1}$  in LB is assigned as a  $b_{3u}$  C—H out-of-plane deformation of the benzenoid groups. The mode at  $1284\text{ cm}^{-1}$  in LB is due to a  $b_{1u}$  benzenoid-amine stretching vibration. The large vibrational mode at  $1497\text{ cm}^{-1}$  in LB results from a  $b_{1u}$  C—C ring-stretching mode. The relatively weak mode as  $1613\text{ cm}^{-1}$  is likely a disorder-induced  $a_g$  C—C ring-stretching mode.

In EB, two new modes are present at 1166 and  $1592\text{ cm}^{-1}$  that correspond to two strong Raman modes of LB (Ref. 28) at 1188 and  $1623\text{ cm}^{-1}$ . The  $1166\text{-cm}^{-1}$  mode is assigned as either an  $a_g$  C—H in-plane ring deformation or an  $a_g$  ring-amine-stretching vibration. These normally infrared-*inactive* modes become infrared *active* when different substituents (amine nitrogens or imine nitrogens) are placed in positions 1 and 4 of the *para*-disubstituted benzenes,<sup>29</sup> resulting in broken symmetry along the chain. The  $1592\text{-cm}^{-1}$  mode has two sources: a C—C ring stretching vibration of the quinoid groups and an  $a_g$  C—C ring stretching mode of the benzenoid groups (as in LB, but much stronger). Again, the symmetry-breaking role of the quinoid groups present in EB causes the Raman mode to become ir active. The relative intensity of the two modes at 1166 and  $1592\text{ cm}^{-1}$  can be used as a measure of the oxidation state (i.e., the number of quinoid groups) in polyaniline between LB ( $1-y=0$ ) and PNB ( $1-y=1$ ).

## B. Photoinduced absorption

### 1. Emeraldine base

The similarity of the near-steady-state photoinduced-absorption spectra of EB for 2.54- and 3.8-eV pumping (Fig. 4) and of the long time photoinduced-absorption spectra of EB for 2.0-, 2.54-, and 3.8-eV pumping (Figs. 10 and 11) suggests that the same types of photoinduced defect states are created for all of these pump energies. The near-steady-state PA features in EB at 1.4 and 3.0 eV have been previously assigned to the formation of positive polarons  $P^+$ ,<sup>10</sup> while the origin of the lower PA peak at 0.9 eV has been unclear to this point. The PB peak at 3.7 eV is due to bleaching of the interband ( $\pi$ - $\pi^*$ ) transition due to formation of polarons.

The PB peak at 1.9 eV results primarily from the creation of excitons involving the quinoid rings. This as-

ignment is consistent with pump-intensity-dependent measurements that indicate that the magnitude of the 1.9-eV exciton (quinoid) bleaching peak scales linearly with pump intensity for 2.54-eV pumping,<sup>10</sup> but sub-linearly ( $I^{0.7}$ ) for 3.8-eV pumping (see Fig. 5). For 2.54-eV pumping, the linear dependence results from the direct photoproduction and recombination of excitons through a unimolecular decay process. For 3.8-eV pumping, the sublinear dependence suggests the admixture of bimolecular recombination decay processes resulting from photoproduction of separating electron-hole pairs. The bleaching of the exciton peak indicates that the formation of polarons involves the quinoid sites, thereby reducing the number of available exciton states.

For 3.8-eV pumping, the other PA peaks at 0.9, 1.4, and 3.0 eV in EB depend on the pump intensity as  $I^{0.6}$  to  $I^{0.7}$ , in contrast to 2.54-eV pumping ( $I^{0.5}$ ),<sup>10</sup> which again suggests a more complicated decay process due to the presence of additional photogenerated electrons and holes. The chopper-frequency dependence of all peaks (see Fig. 6) varies as  $f^{-0.1}$  to  $f^{-0.3}$ . In particular, the 1.4-eV peak shows a stronger frequency dependence than that of the 0.9-eV peak, indicating that the 1.4-eV peak dominates the PA spectrum at long times, consistent with the long time PA spectrum of EB shown in Fig. 10.

In the long time experiment, the 1.4-eV ( $11\,200\text{ cm}^{-1}$ ) PA peak is present, while the 0.9-eV peak, seen in the near-steady-state experiment, is absent or is hidden under the long tail to the mid-ir region (Fig.10). The photoinduced IRAV modes are clearly present, but are much weaker than the 1.4-eV absorption. Both the 1.4-eV peak and the IRAV modes are very long lived, having been observed at times greater than 2 h after photoexcitation when the sample is held at  $\sim 80$  K. The PA spectra for 2.54- and 3.8-eV pumping are virtually identical apart from some minor differences in oscillator strengths and the region of crossover to photoinduced bleaching. Differences in the higher energy crossover can be explained due to instrumental drift of the FTIR spectrometer in this very sensitive, short-wavelength region.

The photoinduced IRAV spectra of EB (Fig. 11) show two PA features at  $1144$  and  $1574\text{ cm}^{-1}$  that are associated with symmetry breaking of *para*-disubstituted benzene rings along the polymer backbone in which formerly Raman-active modes become ir active.<sup>8,9</sup> The two PB features at  $1510$  and  $1599\text{ cm}^{-1}$  indicate a change in the benzenoid and quinoid character of a fraction of the rings. The photoinduced IRAV modes in EB are virtually identical (within the noise level) for all three pump energies, which demonstrates that the same type of long-lived charged defect is formed upon photoexcitation at 2.0, 2.54, and 3.8 eV. Other small photoinduced IRAV modes appear around  $850\text{ cm}^{-1}$  and in the range  $1200$ – $1400\text{ cm}^{-1}$  indicating the sensitivity of other vibrations to the presence of charged defects.

### 2. Leucoemeraldine base

The near-steady-state PA spectra of LB, shown in Fig. 7, reveal two strong PA peaks at 0.75 and 2.8 eV and, in addition, a strongly chopper-frequency-dependent peak

at  $\sim 1.4$  eV. Because of the presence of similar photoinduced-absorption peaks in EB, it appears that similar defect states are photogenerated in LB.

In EB the presence of the PB peak at 1.9 eV is attributed primarily to the creation of excitons involving the quinoid rings. In the absence of quinoid groups (as in fully reduced LB), no bleaching is expected. In our samples of LB, titration studies and uv/visible/near-ir spectra give evidence for a small percentage ( $\sim 3-4\%$ ) of quinoid rings so that the presence of the PB peak in 1.9 eV is not surprising. Initial PA studies of PPS (which is stable in air, is isostructural to LB, and possess no residual oxidized, or quinoidlike, units) show similar PA peaks near 0.85 and 3.1 eV, with no PB peak at intermediate energies.<sup>30</sup>

The PA spectrum of LB was studied as a function of pump intensity and chopper frequency (see Figs. 8 and 9). All of the PA and PB peaks scale as the square root of the pump intensity, suggesting that the excitations responsible for each of these features decay by a bimolecular recombination process. The pump beam chopper-frequency dependences of the PA peaks at 0.75 and 2.8 eV are very similar, varying approximately as  $f^{-0.2}$ . The 1.9-eV bleaching peak is found to have nearly the same frequency dependence ( $f^{-0.2}$ ) at low frequencies, but at higher chopping rates, this peak has a stronger dependence, viz.,  $f^{-0.3}$ . The 1.4-eV absorption peak apparently has a strong frequency dependence at low frequencies varying as  $f^{-0.3}$ , with almost no frequency dependence above 20 Hz. With the size of the 1.4-eV PA peak increasing rapidly below 20 Hz, one might expect the 1.4-eV feature to dominate in the long time experiment. Indeed, our results shown in Fig. 12 indicate that this peak is the dominant one at long times.

The overall intensity of the PA spectrum of LB in the long time experiment is much smaller than that of EB. In particular, the 1.4-eV peak is about 6 times weaker, whereas the photoinduced IR/V modes are  $\sim 3$  times weaker. Because EB contains  $\sim 25\%$  quinoid rings, the size of the 1.4-eV peak in LB is consistent with a six-fold decrease in the number of quinoid rings in our samples. A peak corresponding to the 0.75-eV peak in LB may also be present in EB (near 0.9 eV), but because of the dominance of the 1.4-eV peak it is not observed in the long time experiment.

The photoinduced IR/V spectrum of LB, shown in Fig. 13, shows two PA features at 1144 and 1574  $\text{cm}^{-1}$  that correspond (as in EB) to symmetry breaking of *para*-disubstituted benzene rings on the polymer backbone. The PB mode at 1510  $\text{cm}^{-1}$  indicates, just as in EB, a small decrease in the number of benzene rings. Comparing the PB in EB at 1599  $\text{cm}^{-1}$  to that in LB, we see that any bleaching of this quinoid vibration is below our detection limits for the very few quinoid rings in LB.

## V. PROPOSED MODEL

To explain the origin of the photoinduced-absorption spectra we propose a model that describes the ground-state and excited-state properties of polyaniline. In this model, we start with the ground state of leucoemeraldine

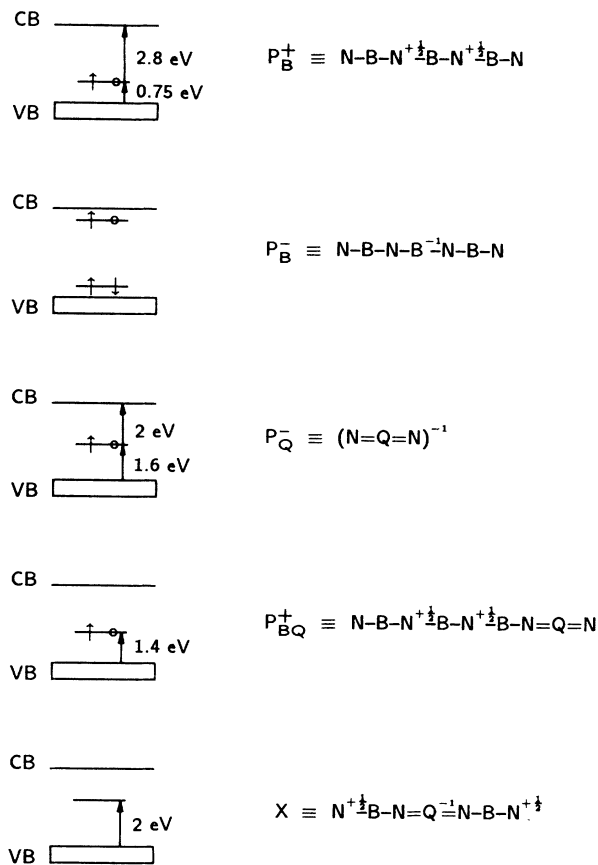


FIG. 14. Schematic definition of defect states  $P_B^+$ ,  $P_B^-$ ,  $P_Q^-$ ,  $P_{BQ}^+$ , and  $X$  with approximate energy level diagrams.  $B$  denotes a benzenoid ring,  $Q$  a quinoid ring, and  $N$  represents either an amine nitrogen (adjacent to two  $B$ 's) or an imine nitrogen (adjacent to a  $Q$ ). Note that the charge distributions of the defects are expected to be more delocalized than those schematically shown here for simplicity. The splitting for  $P_B^-$  is expected to be no more than a few tenths of an eV.

base and consider the removal, addition, or rearrangement of electrons through oxidation, reduction, or photoexcitation. Several excited states discussed in this section are schematically represented in the text and in Fig. 14. They include (1) the hole polaron  $P_B^+ \equiv N-B-N^{+1/2}-B-N^{+1/2}-B-N$ ; (2) the electron polaron  $P_B^- \equiv N-B-N-B^{-1}-N-B-N$ ; (3) the negative polaron trapped at a quinoid (negatively charged quinoid)  $P_Q^- \equiv (N=Q=N)^{-1}$ ; (4) a hole polaron trapped near a quinoid  $P_{BQ}^+ \equiv N-B-N^{+1/2}-B-N^{+1/2}-B-N=Q=N$ ; and (5) the exciton  $X \equiv N^{+1/2}-B-N=Q^{-1}-N-B-N^{+1/2}$ . In this notation,  $B$  represents a benzenoid site ( $=C_6H_4-$ ),  $Q$  a quinoid site ( $=C_6H_4=$ ), and  $N$  represents either an *amine* nitrogen (i.e.,  $N-H$ ) if adjacent to  $B$ , or an *imine* nitrogen (no H) if adjacent to  $Q$ . In addition, the charges will be more delocalized than indicated in these notations. In all of these excited-state configurations, it is expected from theoretical calculations<sup>14,15,24,25,31</sup> that ring-angle distortions and bond-

length changes are important.

Recent calculations<sup>15</sup> utilizing a Hückel Hamiltonian describe the ground state of LB in terms of ring-rotational parameters. The ground-state configuration consists of adjacent phenyl rings twisted out of the nitrogen-nitrogen plane by equal but opposite angles, viz.,  $\psi_0 \approx \pm 56^\circ$  [Fig. 15(a)]. Changes in the number of electrons along the polymer backbone result in new ring angles different from the ground-state configuration.

The removal of an electron from LB results in the formation of a hole polaron,  $P_B^+$ , described as a ring-centered distortion in which the center phenyl ring twists out of its ground-state configuration *toward* the plane formed by the nitrogens. The distortion also causes neighboring rings to distort toward planarity and away from the ground-state angle; see Fig. 15(b). The resulting configuration costs some steric energy, but the  $\pi$  delocalization energy, which favors a planar ring conformation, increases.

Because of non-charge-conjugation symmetry in polyaniline, as evidenced by the shape of the valence and conduction bands, the calculations<sup>15</sup> predict that the energy levels of a  $P_B^+$  split off from the valence band by  $\sim 0.75$  eV, with little or no splitting from the conduction band. Thus, one would expect two new absorptions in the gap: a transition from the valence band to the new polaron level and one from this new state to the conduction band (Fig. 14). Our results for the photoinduced-absorption spectrum of LB show two absorptions at  $\sim 0.75$  eV and  $\sim 2.8$  eV that are consistent with this defect level scheme. Both of these absorptions have similar dependences on pump intensity (Fig. 8) and chopper frequency (Fig. 9).

The presence of the ring-rotational polaron  $P_B^+$  in LB will also cause changes in the infrared spectrum. Infrared absorption data of LB can be interpreted in terms of normal modes of *para*-disubstituted benzene.<sup>8,9,27</sup> The Raman spectrum of LB (Ref. 28) consists of two strong  $a_g$  modes at 1188 and 1623  $\text{cm}^{-1}$  present in *para*-disubstituted benzenes. With a  $P_B^+$  on the ideal LB

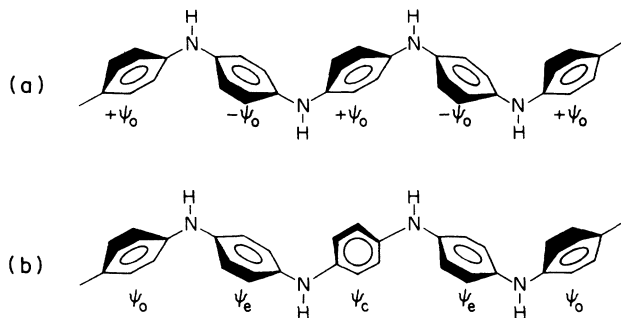


FIG. 15. (a) Sketch of a segment of a leucoemeraldine base chain showing the phenyl rings rotated by  $\pm\psi_0$  out of the plane formed by the nitrogens. (b) Representation of a ring-rotational hole polaron in LB where the center phenyl ring and the end phenyl rings rotate toward the nitrogen plane to new ring angles  $\psi_c$  and  $\psi_e$ .

chain, the symmetry of the chain is broken causing the Raman modes to become ir active. These new modes are observed in oxidative doping studies<sup>8,9</sup> and in the photoinduced ir data at 1144 and 1574  $\text{cm}^{-1}$ , shown in Fig. 13. In addition, the symmetry breaking reduces the number of *para*-disubstituted benzene rings, causing a bleaching of the mode at 1510  $\text{cm}^{-1}$ .

Preliminary calculations<sup>15</sup> suggest that a negative polaron  $P_B^-$  in LB causes almost no ring-rotational effects, although bond-length effects produce very small asymmetrical splittings from the conduction and valence bands, perhaps less than a few tenths of an eV (see Fig. 14). New absorptions arising from this state may be difficult to observe, although similar changes in the infrared modes as observed for the  $P_B^+$  defect would be expected.

Our samples of LB are known to contain a few quinoid rings whose neighboring nitrogen atoms have no hydrogens attached. A quinoid ring can be viewed as a neutral bipolaron, i.e., 2 electrons removed from the  $\pi$  system and compensated for by the removal of protons, which results in a new lattice configuration with the newly formed quinoid ring being planar (or nearly so),<sup>24,25</sup> in addition to the appropriate bond-length changes. A new, localized energy level at  $\sim 2$  eV above the valence band is formed, which then gives rise to the 2-eV “exciton” absorption involving charge transfer from neighboring benzenoid rings to the quinoid ring.<sup>5,24,25</sup> This exciton formation leaves the quinoid ring with a net negative charge and the neighboring benzenoid rings with a net positive charge. A reorganization of ring angles and bond lengths follows as a consequence of the new electronic configuration.<sup>24</sup> The exciton and its energy level diagram are shown schematically in Fig. 14.

The quinoid ring on the polymer backbone is expected to cause changes in the infrared spectrum that are similar to those caused by polarons, i.e., new modes appearing at  $\sim 1150$  and  $\sim 1600$   $\text{cm}^{-1}$ . For our LB samples, the concentration of quinoids is quite small so that very little ir activity is observed at these energies. However, as one allows oxidation of LB samples towards EB, new modes do appear.<sup>9</sup> As noted above, there is a normal mode of the quinoid ring at  $\sim 1600$   $\text{cm}^{-1}$  that overlaps the broken-symmetry mode.

The quinoid site is expected to serve as an electron trap.<sup>24,25</sup> Upon photoexcitation of electron-hole pairs, an electron removed from a benzenoid ring (excited by 3.8-eV pumping) could be captured by a quinoid ring. This trapped electron removes the “exciton” absorption level from the available density of states and, hence, bleaches that absorption band, consistent with our results. We label this quinoid-bound electron site as  $P_Q^-$ , shown schematically in Fig. 14. The electronic transitions of the  $P_Q^-$  (Fig. 14) reflect the expected shift of the quinoid energy level upon occupation of an electron.<sup>25</sup> Strong bleaching of the “exciton” transition, which overlaps the transitions of the  $P_Q^-$ , may make direct observation of the  $P_Q^-$  difficult. The  $P_Q^-$  also causes a change in the bond lengths of the quinoid ring, which is revealed as a PB peak at 1599  $\text{cm}^{-1}$  in the mid-ir PA spectrum of EB.

Our picture thus far explains the presence of the two PA peaks in LB at 0.75 and 2.8 eV due to the presence of

hole polarons. Coulomb interactions may cause the lower PA peak to shift to slightly higher energies at 0.9 eV in EB. If the lower PA peak (at 0.75 eV in LB and 0.9 eV in EB) is an intrinsic signature of a  $P_B^+$ , what is the origin of the 1.4-eV PA peak? In the original PA experiments on EB,<sup>10</sup> the 1.4-eV peak was assigned to the presence of photogenerated polarons based upon a corresponding peak at  $\sim 1.5$  eV due to polarons in emeraldine salt. There have been several reports of the optical absorption in ES that reveal absorption peaks near 1.0 and/or 1.5 eV.<sup>2,32-34</sup> The variability with experiment may be due to differences in preparation conditions, crystalline structure, oxidation state, and protonation conditions.

We suggest that the 1.4-eV photoinduced-absorption peak may result from a bound state of the hole polaron and a nearby quinoid ring, consistent with calculations by Stafström *et al.*<sup>25</sup> If a  $P_B^+$  is located near a planar (or nearly planar) quinoid ring,  $\pi$  holes will delocalize over several lattice sites without having to drive additional rings toward planarity. The gain in delocalization energy may be enough to bind or trap a  $P_B^+$  near a quinoid site. This bound-state configuration, which we denote  $P_{BQ}^+$ , and its energy level diagram are shown schematically in Fig. 14. The 1.4-eV absorption is expected to be strong, while the other at  $\sim 2.2$  eV is weak.<sup>25</sup> The  $P_{BQ}^+$  may take a longer time to form since the ring-rotational polaron must travel to a region containing a quinoid site, and in LB any quinoid rings should be well separated. In addition, once formed, the  $P_{BQ}^+$  would be expected to be long-lived because of the large inertial mass involved for diffusion and thus recombination. The very small 1.4-eV peak at higher chopper frequencies (short times) and the strong low chopper-frequency (long time) behavior in the near-steady-state experiments, as well as the long-lived behavior in the long time experiments, support this assignment.

In addition to the 1.4-eV peak in EB, Stafström *et al.* predict a 3.0-eV PA peak due to transitions from a lower-lying electronic band to the  $P_{BQ}^+$  level.<sup>25</sup> The similar pump intensity dependence (Fig. 5) and chopper-frequency dependence (Fig. 6) of these two peaks is consistent with the expected dominance of transitions to the  $P_{BQ}^+$  state because of the large number of quinoid rings (ideally, every fourth ring) in EB. This signature contrasts that observed in LB where the  $P_B^+$ 's are dominant, and the 0.75- and 2.8-eV peaks behave similarly.

The dominance of the  $P_{BQ}^+$  signature in EB is also observed in the long time experiment, which shows virtually no absorption near 0.9 eV, with a very strong absorption at 1.4 eV. The long lifetime of this latter peak at low temperature<sup>8,9</sup> may result from the inability of the  $P_B^+$ 's, the  $P_{BQ}^+$ 's, and the  $P_Q^-$ 's, which involve ring rotations and bound electronic states, to recombine and relax back to their original ground-state configuration. At higher temperatures, relaxation should be possible due to larger thermally activated free volume for ring rotations.<sup>19</sup>

The magnitude of the photoinduced IRAV modes in EB is  $\sim 2-3$  times those in LB, while the intensity of the 1.4-eV peak is  $\sim 6$  times larger. The increase in size of the 1.4-eV peak appears to scale with the number of

quinoid rings in the polymer. The IRAV modes do not increase as much because they appear even if no quinoids are present, i.e., their existence depends on distortions of the backbone chain due not only to the presence of quinoids, but also to the presence of  $P_B^+$ 's,  $P_B^-$ 's, and  $P_{BQ}^+$ 's. In EB we observe a bleaching of the quinoid mode at  $1599\text{ cm}^{-1}$  due to a small decrease in the number of (pure) quinoid rings that occurs when the defect states are photoproduced.

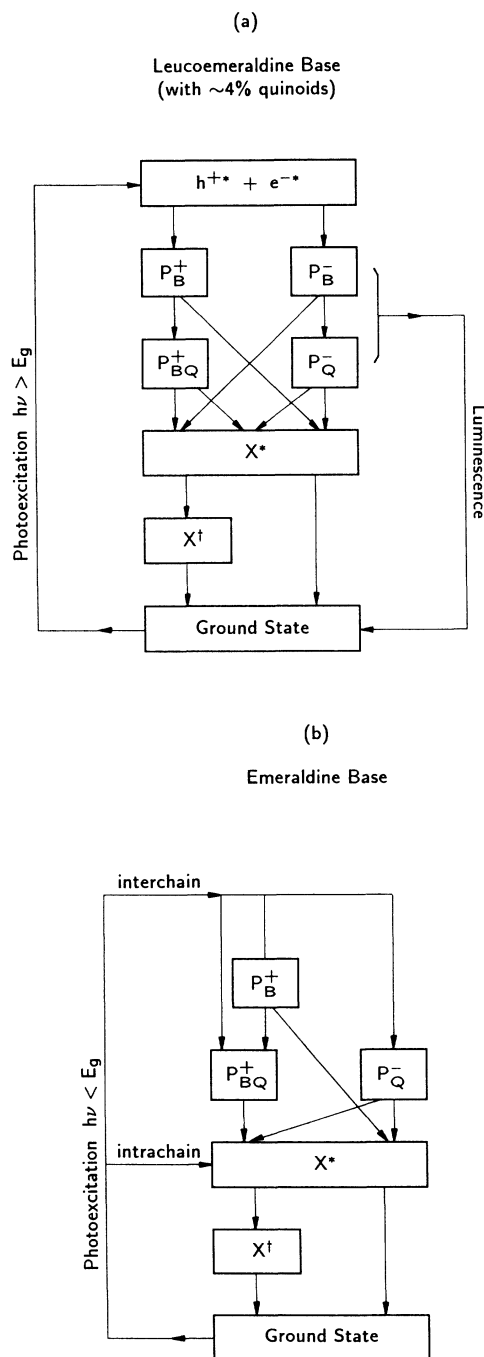


FIG. 16. Schematic representation of a model for photoproduction and relaxation of defect states in (a) LB for above-gap photoexcitation and (b) EB for below-gap photoexcitation.

The presence of photoinduced IRAV modes in EB and LB shows that the infrared modes are sensitive to the configuration of the photoexcited polymer. However, the photoinduced IRAV modes are quite small compared to the higher-lying PA peaks. This signature indicates that the polarons are massive ( $M_{\text{polaron}} > 60m_e$ ) when analyzed in the amplitude mode<sup>35,36</sup> or bond-order polaron<sup>37</sup> formalisms. Theoretical calculations<sup>15</sup> give estimates of  $M_{\text{polaron}}$  for the ring-rotational polarons in LB that are entirely consistent with the long-lived, massive polarons or trapped states observed in these experiments. It is noted that similarly small photoinduced IRAV modes compared to higher-lying photoinduced electronic transitions in pernigraniline base have been observed.<sup>38</sup> These features are long-lived, indicating the presence of massive defect states involving ring rotations in this system as well.

To summarize, Fig. 14 schematically shows each of the defect states that can be created upon photoexcitation of LB containing a few quinoid sites. The hole polaron  $P_B^+$  gives rise to new absorptions at  $\sim 0.75$  and  $\sim 2.8$  eV. The negative polaron  $P_B^-$  will be almost unobservable. The deep-trapped negatively charged quinoid  $P_Q^-$  will be expected to give rise to two photoinduced-absorption peaks near 2 eV, although the bleaching of the "exciton" absorption ( $X$  in Fig. 14) appears to dominate. The trapped state  $P_{BQ}^+$  will yield a new absorption near 1.4 eV. (The second absorption at  $\sim 2.2$  eV is expected to be weak.<sup>25</sup>) In EB we expect that similar defects will be formed for 3.8-eV pumping, although for 2.5-eV pumping all defects except for the  $P_B^-$  will be formed.

In Fig. 16 we present a scheme for the photoproduction and relaxation of defect states in LB containing a few quinoid rings. A very similar scheme is expected for above-gap ( $> 3.6$  eV) photoexcitation of EB, whereas for below-gap photoexcitation some differences are noted. Other effects that may have significant impact on this scheme include interchain interactions, chain ends, crosslinking, and oxidation level.

Photoexcitation of LB above the energy gap creates excited electron-hole pairs, viz.,  $e^{-*}$  and  $h^{+*}$ . The observation of whitish-blue luminescence (at energies less than the energy gap) in these samples indicates that the electron and hole can separate to form lower energy states, which then recombine with an accompanying photoemission. Upon separation, the electron and hole can form positive and negative polarons,  $P_B^-$  and  $P_B^+$ . The  $P_B^-$  can now decay to a  $P_Q^-$  with the electron trapped at a quinoid site. The  $P_B^+$  can move to a region near a quinoid site and form a  $P_{BQ}^+$  trapped state. A few of the negative polarons could combine with some  $P_{BQ}^+$ 's to form an excited state  $X^*$ , which then could decay directly to the ground state or decay to a long-lived metastable configuration  $X^\dagger$  for return to the ground state via thermally activated ring

rotations. The pathway for exciton formation and decay can also occur if a hole polaron  $P_B^+$  combines with a  $P_Q^-$  or if a  $P_{BQ}^+$  combines with a  $P_Q^-$ .

As mentioned above, the excitation and decay scheme for above-gap pumping of EB is expected to be very similar to that of LB. We would, however, expect a larger population of  $P_{BQ}^+$ 's (and almost no  $P_B^+$ 's) because of the large number of quinoids. For below-gap photoexcitation of EB, the excited excitonic state  $X^*$  would be highly populated, followed by relaxation to the ground state or to a long-lived metastable state. Direct photoproduction of hole polarons  $P_B^+$ , bound-state hole polarons  $P_{BQ}^+$ , and deep-trapped electron levels  $P_Q^-$  is expected to occur (likely through interchain charge transfer) followed by relaxation to the excited exciton  $X^*$ , and further relaxation to the ground state or the long-lived state  $X^\dagger$ .

The scheme that we have presented can account for the observed optical and photoinduced optical phenomena in polyaniline, as well as their variation amongst samples. Other experiments, including those at shorter times (microsecond and picosecond)<sup>39</sup> and light-induced electron spin resonance,<sup>11,40,41</sup> are required to test the existence and decay dynamics of these excited states. Application to other ring-containing polymers such as PPS, PPO, and substituted polyanilines will allow for identification based on different substituents and different conformations involving ring angles and bond lengths.

## VI. SUMMARY

In summary, we have investigated the nature of charged defect states in polyaniline through photoinduced absorption studies in the millisecond and long time scales. Our results on emeraldine base and leucoemeraldine base provide further evidence for the existence of long-lived, massive polarons created upon photoexcitation. Ring rotations in these systems give rise to conformations that strongly localize these polarons, inhibiting recombination or relaxation to the ground state. A comparison of our results to theoretical calculations suggests that the intrinsic polaronic signature is observed as photoinduced absorption peaks near 0.75 eV and near 3.0 eV. The PA peak near 1.4 eV is then due to a state resulting from a hole polaron bound to a quinoid ring.

## ACKNOWLEDGMENTS

This work is supported in part by the U.S. Defense Advanced Research Projects Agency through a contract monitored by the U.S. Office of Naval Research and by National Science Foundation (NSF) Grant No. DMR-85-19509.

<sup>1</sup>See, for example, Proceedings of the International Conference on Science and Technology of Synthetic Metals, Santa Fe, New Mexico, 1988, edited by M. Aldissi (Elsevier Sequoia, Lausanne, 1988-1989) [Synth. Met. 27 (1988); 28 (1989); 29

(1989).

<sup>2</sup>S. Stafström, J. L. Brédas, A. J. Epstein, H. S. Woo, D. B. Tanner, W. S. Huang, and A. G. MacDiarmid, Phys. Rev. Lett. 59, 1464 (1987).

- <sup>3</sup>M. C. dos Santos and J. L. Brédas, *Phys. Rev. Lett.* **62**, 2499 (1989).
- <sup>4</sup>J. M. Ginder and A. J. Epstein, *Phys. Rev. Lett.* (to be published).
- <sup>5</sup>A. J. Epstein, J. M. Ginder, F. Zuo, R. W. Bigelow, H. S. Woo, D. B. Tanner, A. F. Richter, W. S. Huang, and A. G. MacDiarmid, *Synth. Met.* **18**, 303 (1987).
- <sup>6</sup>J. M. Ginder, A. F. Richter, A. G. MacDiarmid, and A. J. Epstein, *Solid State Commun.* **63**, 97 (1987); *Bull. Am. Phys. Soc.* **31**, 582 (1986).
- <sup>7</sup>F. Zuo, M. Angelopoulos, A. G. MacDiarmid, and A. J. Epstein, *Phys. Rev. B* **36**, 3475 (1987).
- <sup>8</sup>R. P. McCall, J. M. Ginder, M. G. Roe, G. E. Asturias, E. M. Scherr, A. G. MacDiarmid, and A. J. Epstein, *Phys. Rev. B* **39**, 10 174 (1989).
- <sup>9</sup>R. P. McCall, M. G. Roe, J. M. Ginder, T. Kusumoto, A. J. Epstein, G. E. Asturias, E. M. Scherr, and A. G. MacDiarmid, *Synth. Met.* **29**, E433 (1989).
- <sup>10</sup>M. G. Roe, J. M. Ginder, P. E. Wigen, A. J. Epstein, M. Angelopoulos, and A. G. MacDiarmid, *Phys. Rev. Lett.* **60**, 2789 (1988).
- <sup>11</sup>Y. H. Kim, S. D. Phillips, M. J. Nowak, D. Speigel, C. M. Foster, G. Yu, J. C. Chiang, and A. J. Heeger, *Synth. Met.* **29**, E291 (1989); Y. H. Kim, C. Foster, J. Chiang, and A. J. Heeger, *ibid.* **26**, 49 (1988).
- <sup>12</sup>F. Zuo, R. P. McCall, J. M. Ginder, M. G. Roe, J. M. Leng, A. J. Epstein, G. E. Asturias, S. P. Ermer, A. Ray, and A. G. MacDiarmid, *Synth. Met.* **29**, E445 (1989).
- <sup>13</sup>R. P. McCall, J. M. Ginder, A. J. Epstein, and A. G. MacDiarmid (unpublished).
- <sup>14</sup>C. B. Duke, A. Paton, E. M. Conwell, W. R. Salaneck, and I. Lundstrom, *J. Chem. Phys.* **86**, 3414 (1987).
- <sup>15</sup>J. M. Ginder, A. J. Epstein, and A. G. MacDiarmid, *Solid State Commun.* **72**, 987 (1989); J. M. Ginder, A. J. Epstein, and A. G. MacDiarmid (unpublished).
- <sup>16</sup>S. Stafström and J. L. Brédas, *Synth. Met.* **14**, 297 (1986).
- <sup>17</sup>D. S. Boudreaux, R. R. Chance, J. F. Wolf, L. W. Shacklette, J. L. Brédas, B. Thémas, J. M. André, and R. Silbey, *J. Chem. Phys.* **85**, 4584 (1986).
- <sup>18</sup>J. J. Langer, *Synth. Met.* **20**, 35 (1987).
- <sup>19</sup>S. Kaplan, E. M. Conwell, A. F. Richter, and A. G. MacDiarmid, *Macromolecules* **22**, 1669 (1989); *Synth. Met.* **29**, E235 (1989); *Polym. Prepr.* **29**, 58 (1988).
- <sup>20</sup>A. G. MacDiarmid, J. C. Chiang, A. F. Richter, N. L. D. Somasiri, and A. J. Epstein, in *Conducting Polymers*, edited by L. Alcácer (Reidel, Dordrecht, The Netherlands, 1987), p. 105.
- <sup>21</sup>A. Ray, G. E. Asturias, D. L. Kershner, A. F. Richter, A. G. MacDiarmid, and A. J. Epstein, *Synth. Met.* **29**, E141 (1989).
- <sup>22</sup>M. E. Jozefowicz, R. Laversanne, H. H. S. Javadi, A. J. Epstein, J. P. Pouget, X. Tang, and A. G. MacDiarmid, *Phys. Rev. B* **39**, 12 958 (1989).
- <sup>23</sup>G. E. Asturias, A. G. MacDiarmid, R. P. McCall, and A. J. Epstein, *Synth. Met.* **29**, E157 (1989).
- <sup>24</sup>C. B. Duke, E. M. Conwell, and A. Paton, *Chem. Phys. Lett.* **131**, 82 (1986).
- <sup>25</sup>S. Stafström, B. Sjögren, and J. L. Brédas, *Synth. Met.* **29**, E219 (1989).
- <sup>26</sup>B. Sjögren and S. Stafström, *J. Chem. Phys.* **88**, 3840 (1988).
- <sup>27</sup>R. P. McCall and A. J. Epstein (unpublished).
- <sup>28</sup>Y. Furukawa, T. Hara, Y. Hyodo, and I. Harada, *Synth. Met.* **16**, 189 (1986); M. Ohira, T. Sakai, M. Takeuchi, Y. Kobayashi, and M. Tsuji, *ibid.* **18**, 347 (1987).
- <sup>29</sup>G. Varsányi, *Vibrational Spectra of Benzene Derivatives* (Academic, New York, 1969).
- <sup>30</sup>J. M. Ginder, R. P. McCall, J. M. Leng, and A. J. Epstein (unpublished).
- <sup>31</sup>S. Stafström, *Synth. Met.* **18**, 387 (1987).
- <sup>32</sup>R. J. Cushman, P. M. McManus, and S. C. Yang, *J. Electroanal. Chem.* **291**, 335 (1986).
- <sup>33</sup>Y. Cao, P. Smith, and A. J. Heeger, *Synth. Met.* **32**, 263 (1989).
- <sup>34</sup>K. Kim, J. M. Ginder, J. M. Leng, R. P. McCall, A. J. Epstein, E. M. Scherr, and A. G. MacDiarmid (unpublished).
- <sup>35</sup>E. Ehrenfreund, Z. Vardeny, O. Brafman, and B. Horovitz, *Phys. Rev. B* **36**, 1535 (1987); Z. Vardeny, E. Ehrenfreund, O. Brafman, A. J. Heeger, and F. Wudl, *Synth. Met.* **18**, 183 (1987).
- <sup>36</sup>B. Horovitz, *Solid State Commun.* **41**, 729 (1982).
- <sup>37</sup>M. J. Rice and S. R. Phillpot, *Phys. Rev. Lett.* **58**, 937 (1987).
- <sup>38</sup>J. M. Ginder, R. P. McCall, J. M. Leng, H. J. Ye, Y. Sun, S. K. Manohar, A. G. MacDiarmid, and A. J. Epstein (unpublished).
- <sup>39</sup>M. G. Roe, J. M. Ginder, T. L. Gustafson, A. Angelopoulos, A. G. MacDiarmid, and A. J. Epstein, *Phys. Rev. B* **40**, 4187 (1989).
- <sup>40</sup>M. G. Roe, J. M. Ginder, R. P. McCall, K. R. Cromack, A. J. Epstein, T. L. Gustafson, M. Angelopoulos, and A. G. MacDiarmid, *Synth. Met.* **29**, E425 (1989).
- <sup>41</sup>K. R. Cromack, J. M. Ginder, A. J. Epstein, and A. G. MacDiarmid (unpublished).